7.3 EFFECTS OF HELIUM-DPA INTERACTIONS ON CAVITY EVOLUTION IN TEMPERED MARTENSITIC STEELS UNDER DUAL ION-BEAM IRRADIATION - Takuya Yamamoto, Yuan Wu, G. Robert Odette (University of California Santa Barbara), Sosuke Kondo, Akihiko Kimura (Kyoto University)

OBJECTIVE

The objective of this research is to characterize how cavity and other microstructural evolution in irradiated candidate ferritic and martensitic structural alloys are influenced by the starting microstructure and irradiation variables, including displacements per atom (dpa), dpa rate and the helium/dpa (He/dpa) ratio.

SUMMARY

Cavity evolution in normalized and tempered martensitic steel (TMS) F82H under Fe^{3+} and He^{+} dual ion beam irradiation (DII) at 500°C was characterized over a wide range of dpa, He and He/dpa. Transmission electron microscopy (TEM) showed that DII up to ≈ 60 dpa and ≈ 2400 appm He produced a significant population of non-uniformly distributed cavities with bimodal sizes, ranging from ≈ 1 nm He bubbles to ≈ 20 nm faceted voids, resulting in observed swelling of up more than 3%. The incubation dpa for the onset of void swelling decreased linearly with increasing He/dpa in both IEA and mod.3 heats of F82H.

BACKGROUND

Predicting and mitigating the effects of a combination of large levels of transmutant He and displacement damage (dpa), produced by high energy neutrons, on the dimensional stability and mechanical properties of structural materials is one of the key grand challenges in the development of fusion energy [1]. The fundamental overriding questions about He and dpa effects and their synergisms include: a) what are the basic interacting mechanisms controlling He and displacement defect transport, fate and consequences; b) how are the resulting cavity and other evolutions influenced by the starting microstructure and irradiation variables, including, displacements per atom (dpa), dpa rate, He/dpa ratio and irradiation temperature; and, c) how can the detrimental effects of He-dpa synergisms be mitigated and managed by proper microstructural designs?

We have previously demonstrated that in situ He implantation (ISHI) in mixed spectrum fission reactor irradiations provides a very attractive approach to assessing the effects of He-dpa synergisms, while avoiding most of the confounding effects associated with Ni- or B-alloy doping type experiments [1-8]. Another approach is to use dual ion beam irradiations (DII) to simultaneously implant He and produce displacement damage [1,9-12]. Note, the two techniques are complementary, but manifest many differences that, in the case of DII, include: a) much higher dpa rates; b) non-uniform spatial distributions of dpa and He; and, c) the proximity of a free surface. Notably, the spatial variations of He and dpa in DII permits assessing the effects of a wide range of He and dpa conditions as they vary with ion penetration depth. Over the last five years we have carried out 8 DII studies at 500°C in DuET facility in Kyoto University at various nominal He/dpa and dpa rates (defined at the depth of 600 nm) in F82H Mod.3 and at subset of conditions in F82H IEA with and without cold work. In this report we focus on the growing database on DII cavity evolution (and swelling) trends in F82H Mod.3 encompassing a very wide range of dpa, He and He/dpa. Note that since very similar trends were observed in the as-tempered F82H IEA heat, they are not summarized in this brief report.

Experimental Procedure

The alloys studied were two variants of tempered martensitic steel (TMS) F82H, namely F82H IEA and F82H Mod.3. The F82H alloy series includes several variants of a base 8Cr TMS, widely studied in a variety of irradiation experiments, including those characterizing He effects [1,3,7,11-19]. The F82H Mod.3 variant adjusted the base composition of a large program heat F82H-IEA, by reducing the N and Ti, while increasing Ta (nominal in wt.%, 7.5Cr, 2W, 0.2V, 0.1C, 0.1S,i 0.02, 0.001Ti, 0.1Ta, 14ppm N, bal.

Fe) [13]. The heat treatment schedule was: austenitizing at 1040 °C for 30 min, followed by normalizing (air cooling), with a final tempering treatment at 740°C for 1.5 h. The F82H microstructure consists of packets of fine ≈ 1 μm laths contained in prior-austenite grain sizes of ASTM 9.5 for F82H Mod.3 and size 3 for F82H IEA. F82H also contains a variety of carbide precipitates with a wide range of sizes [14]. The 9Cr class TMS alloys have good unirradiated strength (yield stress ≈ 500 MPa) [13] and toughness (100 MPa√m temperature of T_o ≈ -100°C [19]) properties, and can be fabricated and joined to serve in first wall and blanket structures [13]. Along with other TMS alloys, like Eurofer97, F82H is a reference structural steel for fusion applications. Notably TMS alloys are resistant to swelling at low He levels, but experience: a) irradiation hardening and embrittlement, below about 400 °C; b) irradiation creep over a wide range of temperatures; and, c) high temperature thermal creep and corrosion. A key objective is to establish the T-dpa-He window for TMS. This window may be severely restricted at high fusion relevant He levels.

DII were carried out on 0.2 mm thick 3 mm diameter disks or 0.5 mm thick ≈ 1x20 mm rectangular coupons mechanically- and electro-polished prior to irradiation. The DII were performed in DuET facility located at the Institute of Advanced Energy, Kyoto University in Japan. Here, Fe^{3+} and He^{+} ions are accelerated to 6.4MeV and 1MeV, respectively [20]. Table 1 summarizes nominal He and dpa conditions, at the reference 600 nm depth, that is encompassed by the current database. The irradiations targeted two nominal doses, three He/dpa and two dpa rate conditions. Taking advantages of the varying spatial distributions of dpa and He, we characterized the microstructures over a very wide range of He-dpa, as shown in Figure 1a; Figure 1b shows the corresponding dpa-dpa rates, including the low ISHI conditions in HFIR. The dpa are based on SRIM using the Kinchin-Pease displacement energy of 40 eV [21,22].

TEM on FIBed lift outs was performed on the FEI T20 and Titan instruments in the UCSB Microstructure and Microanalysis Facility. Through focus bright field imaging was used to characterize the cavities. We avoided regions that suffer the effects of surface proximity and injected self-interstitials, respectively..

Table 1. Irradiation conditions analyzed in this report.

Exp ID	TMS Alloys	T (°C)	Nominal Condition (@550-650nm)				Peak He (@1000-1100nm)		
			dpa	He (appm)	He/dpa	dpa/s	dpa	He (appm)	He/dpa
DI10B1	F82H mod.3	500	26	1210	47	5.0×10^{-4}	45	2100	47
DI10B2			9.9	457	46	5.2×10^{-4}	17	795	46
DI10B3			10	480	47	5.1×10^{-4}	18	840	47
DI13A1	F82H mod.3	500	26	390	15	5.1×10^{-4}	44	670	15
DI13B1	F82H mod.3, F82H IEA	500	30	848	29	1.5×10^{-3}	51	1467	29
DI14A1	F82H mod.3, F82H IEA	500	30	1200	45	1.3×10^{-3}	52	2400	45

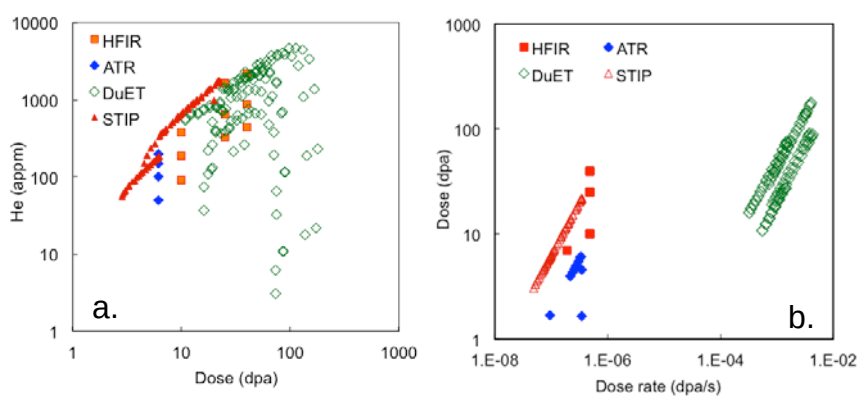

Figure 1. a) A map UCSB irradiation experiments using various techniques, including DII DuET at discrete depth sections: a) a He-dpa map; and, b) a dpa-dpa rate map.

RESULTS

Figure 2a shows a typical cavity microstructure profile from the surface at the left to the depth of ≈ 2 μm at the right. Figure 2b shows the dpa and implanted He as a function of depth over the range shown in Figure 2a. Thin foil energy degraders produced four He ion energy bands with a combined broad concentration peak around ≈ 1.2 μm, shown as the black dashed line. The dpa peaks at ≈ 1.5 μm and reaches a depth of ≈ 2 μm as shown by the red solid line. These two profiles result in an approximately constant He/dpa ratio from ≈ 0.4 to ≈ 1.1 μm, at ≈ 47 appm/dpa in this example, as shown by the green dotted line. The dpe-He profile generally results in cavity number density and sizes that increase with depth up to ≈ 1.2 μm. Figure 2c and 2d compare the cavity microstructures at 0.6 to 0.7 μm. at an average 25 dpa, 1150 appm He and 46 appm/dpa, to those at a depth of 1.1 to 1.2 μm, at 52 dpa, 2060 appm He and 39 appm/dpa. Clearly, larger cavities are found at higher damage levels at the deeper location. This is quantified by the corresponding cavity size distributions shown in Figure 2e. Figures 3a and b show cavity microstructures at a similar dpa ≈ 45 but for a He/dpa ratio of ≈ 15 (Figure 3a) and 47 (Figure 3b), respectively. Figure 3c shows the corresponding cavity size distributions. At lower He/dpa there is a bimodal cavity distribution with peaks at d ≈ 2-2.5 nm and d ≈ 5.5 nm. At the higher He/dpa almost all the bubbles have converted to growing voids peaked at ≈ 5.5 nm. These results are fully consistent with critical bubble models of cavity evolution and void swelling [1]

Swelling Trends

We have quantitatively characterized the cavity evolution trend as a function of dpa, He and He/dpa in terms of their average size, <d>, number density, N, and volume fractions f, previously [23]. Notably <d> and N vary significantly for similar irradiation conditions. This is largely due to the effects of the local microstructure. However, the corresponding variations in f are less. This reflects the fact that variations in the corresponding void $<d_v>$ and N_v are also less, and that the total $f \approx f_v$. Here we assume separation of voids from bubbles at a (≈ critical) size of 4 nm, corresponding to the dip between the two peaks in the cavity size distributions at various conditions.

To date we have collected data on 72 dpa-He-dpa rate DII conditions for F82H Mod.3 and 32 conditions for F82H IEA. Figure 4a shows void volume fraction, f_v, as a function of dpa and He/ dpa ratio in F82H Mod.3. The data show a clear shift of swelling and incubation dpa to lower values with increasing He/dpa. As shown in Figure 4b, a combined damage-dose parameter, dpa* = dpa/[1 + 0.0225 (50 – He/dpa)] collapses the f_v trend at various He/dpa. Figure 4c also shows that the dpa* scaling also collapses the ISHI F82H Mod.3 and Eurofer 97 f_v data at various He/dpa [24]. The ISHI f_v is shifted to lower dpa* compared to the DII cruve indicating a possible dose rate effect. However, more research, especially at higher ISHI dpa and He, is needed to confirm this trend.

Figure 5a shows the corresponding f_v versus dpa plots at various He/dpa in F82H IEA after DII. The data suggest high post incubation swelling rates and swelling levels. The lines are eyeball fits for post-incubation swelling for each of the defined He/dpa groups. Figure 5b shows the dpa at both f_v = 0 (incubation dpa_i) and 1.5%, respectively, decreases linearly with the He/dpa. The swelling rates (slope of the lines) are ≈ 0.11±0.03%/dpa, excluding 5 appmHe/dpa case. This rate is about half of that proposed by Garner for ferritic-tempered martensitic alloys [25]. Figure 4c plots f_v vs. dpa – dpa_i(He/dpa = 30). The f_v do not collapse fully but rather show a trend to higher swelling at lower He/dpa, suggesting that there are secondary effects of He/dpa on the post-incubation swelling behavior. Notably, the swelling levels reach ≈ 3.5%. Even at a nominal He/dpa ≈ 10 appm He/dpa the swelling would reach ≈ 14% at 200 dpa. On the other hand the corresponding swelling is predicted to be minimal at less than 70 dpa. However, dpa rate and other CPI versus DII effects have not been considered in these estimates.

We must close this section with a caveat. The data shown in Figure 5 include different DII runs and intrinsically different regions of the alloy microstructure samples. Thus to the extent that there are small difference in the irradiation conditions and variations background microstructures, these results must be viewed with caution and subject to further verification.

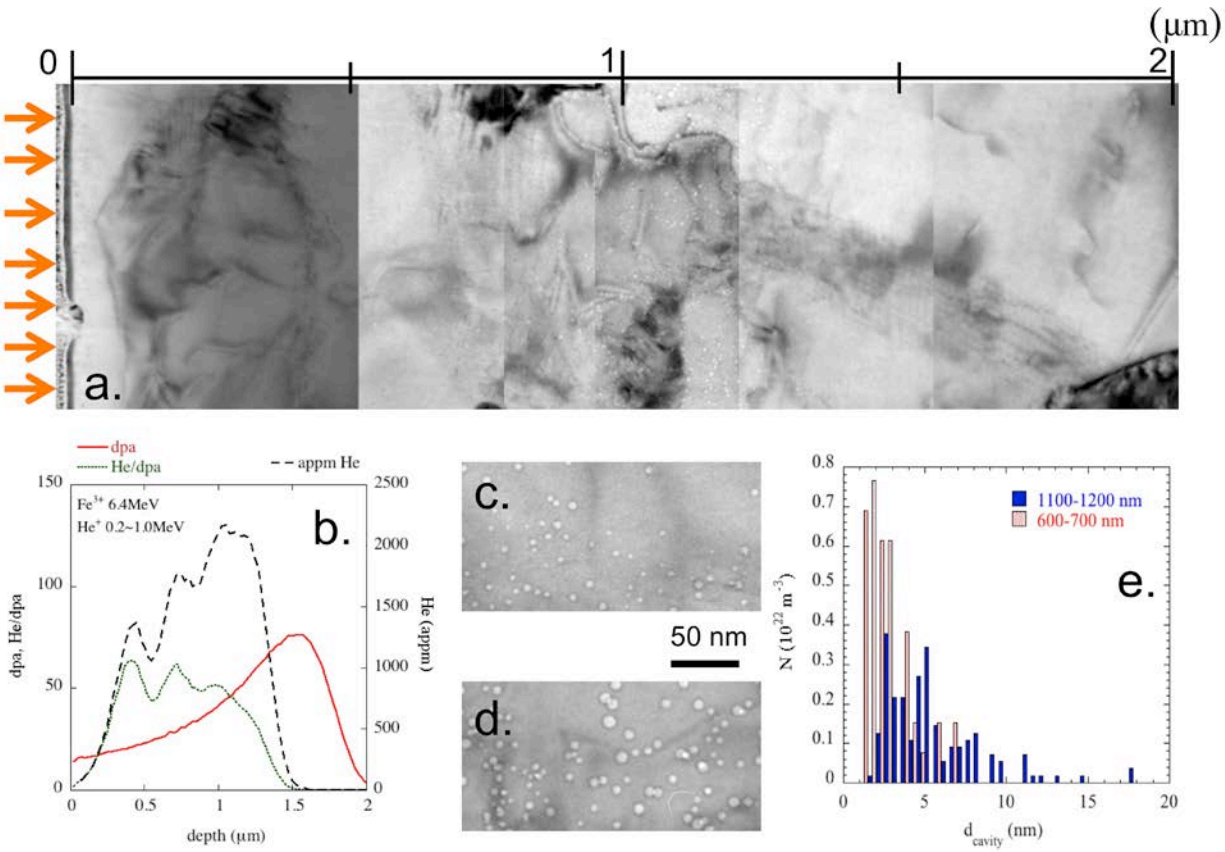

Figure 2. a) The microstructure profile in the DII of F82H Mod.3; b) the dpa (red solid line), He (black dashed line) and He/dpa ratio as functions of depth; c) and d) the cavity microstructures in 0.6 to 0.7 μm and in 1.1 to 1.2 μm sections, respectively; e) the corresponding cavity size distributions.

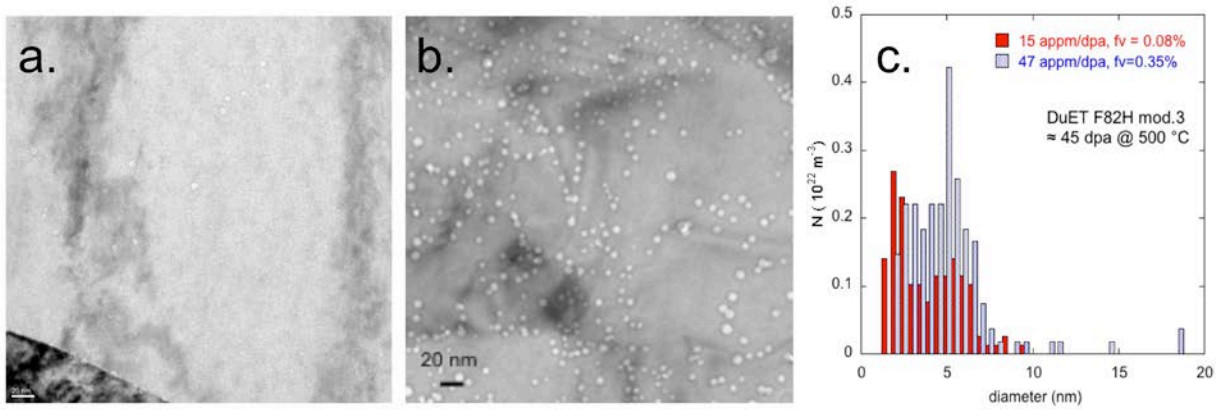

Figure 3. Cavity microstructures in F82H mod. Irradiated at 500°C to ≈ 45 dpa with He/dpa ratios of: a) ≈ 15 and b) ≈ 47 appm He/dpa, respectively; and, c) the corresponding cavity size distributions.

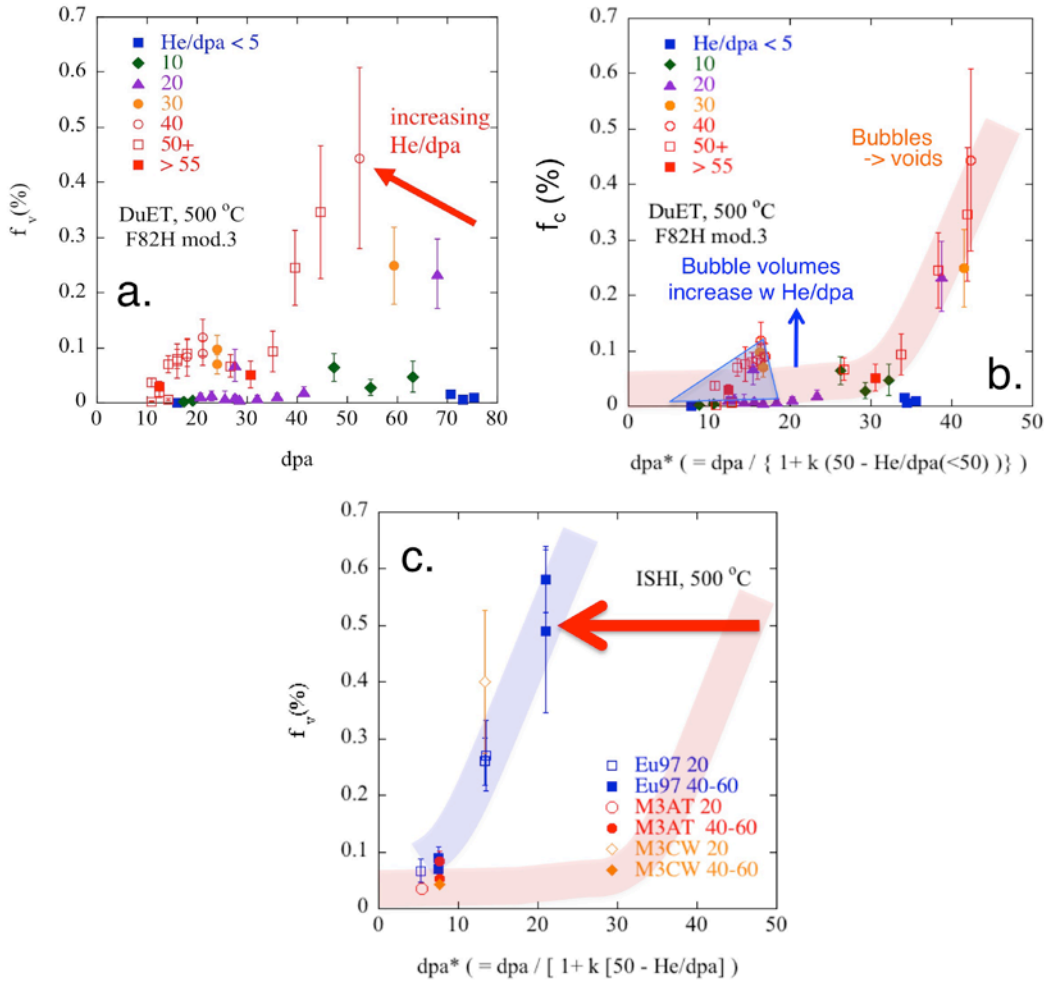

Figure 4. a) The void volume fraction (f_v) versus dpa at various He/dpa ratios in DII F82H Mod. 3; b) the f_v trend on a dpa* scale that collapses He/dpa effects; and, c) f_v versus dpa* in ISHI and DII DuET irradiations.

SUMMARY

Cavity evolutions in normalized and tempered martensitic steel (TMS) F82H under Fe^{3+} and He^{+} dual ion beam irradiations (DII) at 500°C were characterized over a wide range of dpa, He and He/dpa. Transmission electron microscopy (TEM) showed that DII of F82H at 500°C to up to ≈ 60 dpa and ≈ 2400 appm He, produced a moderate number density of non-uniformly distributed cavities with bimodal sizes ranging from ≈ 1 nm He bubbles to ≈ 20 nm faceted voids, and swelling up to ≈ 3.5%. Higher He/dpa systematically accelerates the onset of void swelling and may have a second order effect on rapid post-incubation swelling. Differences between DII and ISHI, including the effects of dpa rate, are critical unresolved issues.

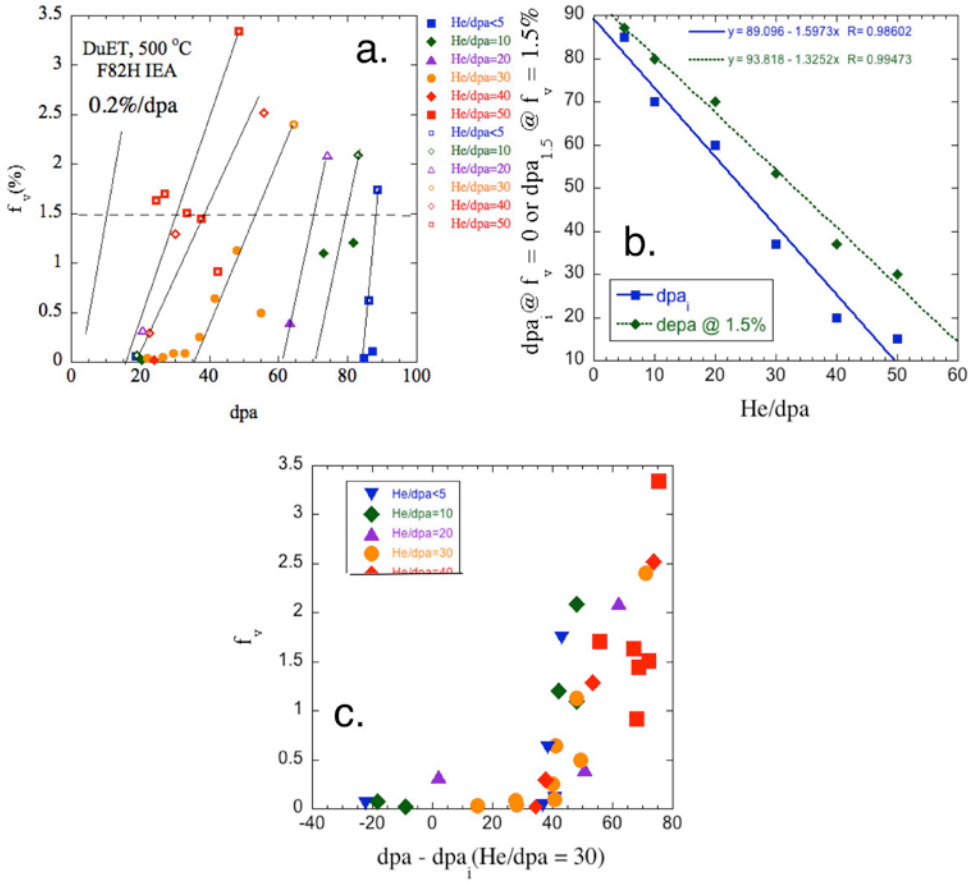

Figure 5. a) Swelling (f_v) as a function of dpa for various He/dpa ratios; b) the dpa at the onset of swelling and f_v = 1.5%; and, c) f_v on a dpa - dpa_i(He/dpa) scale.

ACKNOWLEDGEMENTS

The dual ion-beam irradiations were conducted under the support of the "Joint Research Program on Zero-Emission Energy Research, Institute of Advanced Energy, Kyoto University (ZE26A-16, 25A-19, 24A-13 and 23B-3). The work performed at UCSB was supported by the U. S. Department of Energy, Office of Fusion Energy Sciences, under contract DE-FG03-94ER54275. We acknowledge the contributions of the NSF sponsored UCSB Microstructure and Microanalysis Facility. We are also grateful for generous support of research materials, F82H mod.3 from Dr. K. Shiba, (JAEA, Japan).

REFERENCES

[1] Y. Dai, G.R. Odette, T. Yamamoto, The Effects of helium on irradiated structural alloys, in Comprehensive Nuclear Materials, R. Konings, T. R. Allen, R. E. Stoller, S. Yamanaka Eds. Elsevier (2012).Chap 5

[2] T. Yamamoto, G.R. Odette, L.R. Greenwood, Fusion Materials Semiannual Report 1/1 to 6/30/2005 DOE/ER-313/38 (2005) 95.

[3] T. Yamamoto, G.R. Odette, P. Miao, D.T. Hoelzer, J. Bentley, N. Hashimoto, H. Tanigawa, R. J. Kurtz, J. Nucl. Mater., 367-370 (2007) 399.

[4] R.J. Kurtz, G.R. Odette, T. Yamamoto, D.S. Gelles, P. Miao, B.M. Oliver, J. Nucl. Mater. 367-370 (2007) 417.

[5] G.R. Odette, M.J. Alinger, and B.D.Wirth, Annu. Rev. Mater. Res. 38 (2008) 471.
[6] T. Yamamoto, G.R. Odette, P. Miao et al., J. Nucl. Mater., 386-388 (2009) 338.
[7] D.J. Edwards, R.J. Kurtz, G.R. Odette et al., Fusion Materials Semiannual Report 12/31/2009 DOE/ER-313/47 (2010) 59.
[8] G.R. Odette, P. Miao, D.J. Edwards et al., J. Nucl. Mater., 417 (2011) 1001.
[9] E.H. Lee, J.D. Hunn, T.S. Byun and L.K. Mansur, J. Nucl. Mater. 280 (2000) 18.
[10] H. Kishimoto, K. Yutani, R. Kasada and A. Kimura, Fusion Eng. Des. 81 (2006) 1045.
[11] R. Kasada, H. Takahashi, H. Kishimoto et al., Materials Science Forum 654-656 (2010) 2791.
[12] T. Yamamoto, Y. Wu, G.R. Odette et al., Fusion Materials Semiannual Report 12/31/2010 DOE/ER-313/49 (2011) 1.
[13] K. Shiba, M. Enoeda, S. Jitsukawa, J. Nucl. Mater., 329-333 (2004) 243.
[14] R. Schaublin, P. Spatig, M. Victoria, J. Nucl. Mater., 258-263 (1998) 1178.
[15] A. Kimura, R. Kasada, K. Morishita et al.,,, J. Nucl. Mater., 307-311 (2002) 521.
[16] G.R. Odette, T. Yamamoto, H.J. Rathbun et. al., J. Nucl. Mater., 323 (2003) 313.
[17] T. Yamamoto, G.R. Odette, H. Kishimoto et al., J. Nucl. Mater., 356 (2006) 27.
[18] Z. Tong, Y. Dai, J. Nucl. Mater. 385 (2009) 258.
[19] G.R. Odette, T. Yamamoto, H. Kishimoto et al., J. Nucl. Mater., 329-333 (2004) 1241
[20] A. Kohyama, Y. Katoh, M. Ando and K. Jimbo, Fusion Eng. Des. 51-52 (2000) 789.
[21] ASTM E521-96 (2009), ASTM
[22] R.E. Stoller, M.B. Toloczko, G.S. Was et al., Nuc. Instr. Methods in Phys. Res B 310 (2013) 75.
[23] T. Yamamoto, Y.Wu, G.R. Odette et al, J. Nucl. Mater. 445 1-3 (2004) 190.
[24] G.R. Odette, T. Yamamoto, Y. Wu et al., Fusion Materials Semiannual Report 12/31/2011 DOE/ER-313/51 (2012) 90.
[25] F.A. Garner, M.B. Toloczko, B.H. Sencer, J. Nucl. Mater., 276 (2000) 123.